Geochemistry, Geophysics, Geosystems

RESEARCH ARTICLE
10.1029/2018GC008106

Special Section:
Magnetism in the Geosciences - Advances and Perspectives

Paleomagnetic Secular Variation and Relative Paleointensity During the Holocene in South China—Huguangyan Maar Lake Revisited

Mei Sheng[1,2], Xisheng Wang[1], Mark J. Dekkers[2], Yun Chen[1], Guoqiang Chu[3], Ling Tang[4], Junling Pei[1], and Zhenyu Yang[5]

[1]MNR Key Laboratory of Paleomagnetism and Paleotectonic Reconstruction, Institute of Geomechanics, Chinese Academy of Geological Sciences, Beijing, China, [2]Paleomagnetic Laboratory Fort Hoofddijk, Department of Earth Sciences, Utrecht University, Utrecht, Netherlands, [3]Key Laboratory of Cenozoic Geology and Environment, Institute of Geology and Geophysics, Chinese Academy of Sciences, Beijing, China, [4]Institute of Earth Environment, Chinese Academy of Sciences, Xi'an, China, [5]College of Resources, Environment and Tourism, Capital Normal University, Beijing, China

Key Points:
- A well-dated high-resolution paleomagnetic secular variation record throughout the Holocene from Huguangyan Maar Lake is presented
- This PSV record broadly agrees with typical sediment records from East Asia, Europe, North America, and geomagnetic field model predictions
- This record may be used as a reliable PSV reference curve and a valuable tool for regional correlation and dating purpose in South China

Supporting Information:
- Supporting Information S1
- Data Set S1
- Data Set S2

Correspondence to:
X. Wang,
xishengwang@yahoo.com

Citation:
Sheng, M., Wang, X., Dekkers, M. J., Chen, Y., Chu, G., Tang, L., et al. (2019). Paleomagnetic secular variation and relative paleointensity during the Holocene in South China—Huguangyan Maar Lake revisited. *Geochemistry, Geophysics, Geosystems*, *20*, 2681–2697. https://doi.org/10.1029/2018GC008106

Received 26 NOV 2018
Accepted 29 APR 2019
Accepted article online 6 MAY 2019
Published online 12 JUN 2019

Abstract The scarcity of reliable paleomagnetic secular variation (PSV) records from East Asia especially from low-latitude regions impedes better understanding of global PSV mechanisms. Here we report on a radiocarbon-dated Holocene PSV record from a composite ~6.7-m-long core collected from the high-sedimentation-rate Huguangyan Maar Lake (HML) in subtropical-tropical South China. Rock magnetic results demonstrate that the natural remanent magnetization resides in single-domain magnetite. Alternating field demagnetization experiments at 1-cm spacing on u-channel samples reveal six distinct inclination highs at ~7,500 BCE, ~5,100 BCE, ~4,600 BCE, ~3,600–3,400 BCE, ~1,600–1,200 BCE, and 600–800 CE; three inclination lows at ~4,800 BCE, ~600–300 BCE, and ~1,000–1,300 CE; and three eastward declination trends at ~3,600–3,200 BCE, ~2,600–2,400 BCE, and 400 BCE to 200 CE. The similarity between the HML PSV record and other independently dated records from East Asia and geomagnetic field models corroborates the robustness of our age model and Holocene PSV record. Strikingly, centennial- to millennial-scale PSV features of the HML are comparable, within age uncertainties, with other Holocene records from Europe, North America, and Canada, suggesting that such directional patterns are likely to be hemispheric in scale. Although relative paleointensity data of HML are affected by environmental factors (e.g., organic matter diagenesis), the record still provides a regionally important new PSV reference curve whose conspicuous features may serve as stratigraphic markers for East Asian paleorecords.

1. Introduction

A distribution of paleomagnetic secular variation (PSV) curves as even as possible across the globe during the Holocene is crucial for understanding the dynamics of the Earth's magnetic field over decadal to millennial timescales (Korte & Constable, 2005). Moreover, such curves contribute to high-resolution Holocene stratigraphy and are promising dating tools in archeology (Barletta et al., 2010; Ben-Yosef et al., 2008; Kanamatsu et al., 2017; Lougheed et al., 2014; Lund et al., 2016). During the past decades, Holocene PSV has been extensively studied, which resulted in a substantial number of reliable curves from around the globe, contributing to the establishment and progressive improvements of global geomagnetic field models, such as ARCH3k.1 (Korte et al., 2009), SED3k.1 (Korte et al., 2009), CALS3k.4 (Korte & Constable, 2011), CALS10k.1b (Korte et al., 2011), and pfm9k.1a (Nilsson et al., 2014).

The regional geomagnetic field during the most recent couple of thousands of years is characterized by several sharp directional cusps sometimes referred to as geomagnetic jerks (Gallet et al., 2003; Pavón-Carrasco et al., 2010; Tema & Kondopoulou, 2011). These jerks sometimes coincide with intensity maxima, as documented from Europe (Pavón-Carrasco et al., 2010; Snowball & Sandgren, 2004), West Africa (de Groot et al., 2015; Kissel et al., 2015; Mitra et al., 2013), Middle East (Ben-Yosef et al., 2017; Ertepinar et al., 2012; Shaar et al., 2016), and Hawaii (de Groot et al., 2013; Gonzalez et al., 1997; Mankinen & Champion, 1993; Pressling et al., 2006). Interestingly, the cusps in PSV curves from Korea and Japan in East Asia are nearly identical to the archeomagnetic jerks recorded in the European archeomagnetic data, implying that archeomagnetic jerks were global (or at least Northern Hemispheric) features (Yu, 2012; Yu et al., 2010). Taking

advantage of the longevity of Chinese civilization and abundant archeological artifacts, Cai et al. (2015, 2017, 2014, 2016) established a PSV and archaeointensity reference curve for Eastern Asia spanning the last 8,000 years with materials varying from baked clay, pottery, and porcelain to slag. Additionally, several PSV curves from lake and marine sediments spanning the Holocene in China were also obtained in recent years (Yang et al., 2009, 2012, 2016; Zheng et al., 2014).

Notwithstanding a notable increase in reliable PSV records from the Northern Hemisphere, the distribution of data sets is still distinctly uneven, with a high concentration in the European region but a much lower concentration in East Asia, hampering a better understanding of the global PSV mechanisms. More specifically, in the low latitudinal band (i.e., between the equator and 30°N), only one Holocene sedimentary record from Lake Barombi Mbo in Cameroon, Africa (Thouveny & Williamson, 1988), is included in the GEOMAGIA50.v3 database (Brown et al., 2015), which has an overly large influence on the geomagnetic field models. In the same way, the volcanic and archeological records indexed by the GEOMAGIA50.v3 database (e.g., Donadini et al., 2006; Korhonen et al., 2008; Mitra et al., 2013; Valet et al., 1998) are strongly biased by data paucity in the same low latitudinal band especially from North Africa to East Asia. Thus, high-quality PSV records from low latitudes in East Asia with tight age constraints are urgently needed to construct a reliable master PSV curve for SE Asia and further to improve our knowledge of past geomagnetic field behavior in low latitudes.

Huguangyan Maar Lake (HML; Figure 1), which is situated on the Leizhou Peninsula in the southernmost part of mainland China, is regarded as one of the most complete archives of environmental and climatic change in tropical-subtropical South China since the last glaciation (Mingram et al., 2004; Sheng et al., 2017; Wang et al., 2016; Yancheva et al., 2007). Preliminary rock magnetic study suggests that HML sediments are characterized by strong magnetic signals due to the presence of a large amount of fine-grained magnetite (Duan et al., 2014; Yang et al., 2012). The earlier paleomagnetic results by Yang et al. (2012) demonstrate that the HML PSV record during the Holocene is characterized by three broad peaks in inclination and two broad eastward trends in declination. This was achieved by comparing their HML PSV record with coeval European and North American counterparts. However, the chronological framework of their PSV curve was based mainly on a visual match with PSV records from Northern Hemisphere while their own accelerator mass spectrometry (AMS) ^{14}C data were given less weight, making their PSV curve less convincing. Their age model exhibits an age discrepancy of up to 1,000 years with more recent studies from HML that are deemed more reliable (e.g., Jia et al., 2015; Wang et al., 2016; Wu et al., 2012). Note that their cores were retrieved from the SW margin of the lake where the lake floor is among the steepest portion of the entire lake, as revealed by previous bathymetric measurements (Yancheva et al., 2007). The sedimentary sequence in a sloping lake floor region may well be controlled by very local sedimentary conditions. Specifically, our recent integrated mineral magnetic, pollen, and geochemical analyses reveal that the magnetic signal retrieved from HML is affected by organic matter diagenesis, which may induce dissolution of iron-bearing minerals via iron reduction (Wang et al., 2016). It is therefore critical to assess the effects of organic matter diagenesis on the PSV records. In this study, we revisit this site by high-resolution paleomagnetic analysis based on a new set of cores with precise AMS ^{14}C age control. By detailed comparison with typical high-resolution Holocene PSV records from East Asia and other places in the Northern Hemisphere as well as geomagnetic field models, we aim to (1) evaluate the recording fidelity of PSV and relative paleointensity (RPI) record from HML and (2) attempt to construct a reliable PSV reference curve for stratigraphic correlation and dating purposes in South China. Since the cores are not azimuthally oriented, our record consists of inclinations and RPI with relative declinations associated to it.

2. Background, Materials, and Methods

HML (21°9′N, 110°17′E; Figure 1) is the deepest crater lake of the Leiqiong volcanic field in the southernmost part of mainland China. The bilobate lake, encircled by a high tephra wall and underlain by a basalt sheet, has a diameter of ~1.7 km and a maximum water depth of ~20 m. In September 2011, four parallel cores (A, B, C, and D) were recovered from a water depth of 13.5 m using a high-precession rod-operated corer (Usinger-corer; Mingram et al., 2007). Our coring site and that of Yang et al. (2012) are shown in Figure 1.

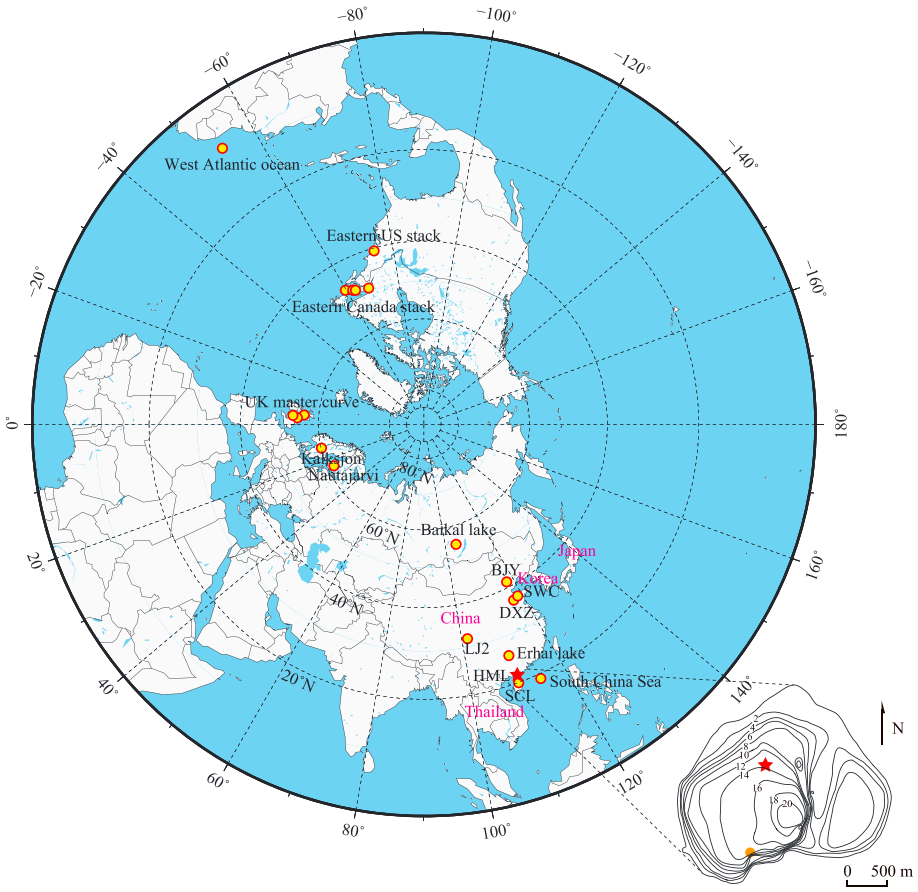

Figure 1. Map of the Northern Hemisphere. The red star indicates the location of Huguangyan Maar Lake (HML). Yellow circles mark other records discussed in this contribution: Baikal Lake in Russia (Peck et al., 1996), Erhai Lake in Yunnan (Hyodo et al., 1999), northern South China Sea (Yang et al., 2016), Shuangchiling (SCL) maar lake in Hainan (Yang et al., 2009), Baojiaying (BJY) in Hebei, Daxinzhuang (DXZ) and Shuangwangcheng (SWC) in Shandong and Liujiazhai (LJZ) in Sichuan (Cai et al., 2016), Lake Kalksjon in Sweden (Stanton et al., 2010; Stanton et al., 2011), Lake Nautajarvi in Finland (Ojala & Tiljander, 2003), the U.K. master curve (Turner & Thompson, 1981), the Demerara Rise in equatorial west Atlantic Ocean (Lund et al., 2017), the eastern U.S. stack (King & Peck, 2001), and the Eastern Canada stack (Barletta, St-Onge, Stoner, et al., 2010). The enlarged figure shows the HML bathymetry (water depth in meter) and locations of our coring site (red star) and that of Yang et al. (2012; orange circle).

A composite 10.6-m-long core from cores B and C spanning the past 20,400 years BP has been built (Sheng et al., 2017; Wang et al., 2016). In this study, we focused on the upper 6.75-m composite core that covers the whole Holocene. Detailed construction of the composite section through comparison of lithology and intensity of natural remanent magnetization (NRM) between cores B and C were presented in the supporting information (Figure S1). The cores were cut in half overlength. One half was sampled by u-channels from the center of the split face of core sections. The top and bottom approximately 1–7 cm of each u-channel were not considered in the analysis to avoid edge effects. Back-to-back discrete samples ($2 \times 2 \times 2$ cm^3 cubes) were collected from the other half core along the center. Water content and dry density were estimated from individual samples at 1-cm intervals (Figure S2). Radiocarbon age dates of 10 plant remains and two charcoal used in this study have been published (Wang et al., 2016). The chronology is further improved by the Bayesian age modeling tool Bacon 2.2 (Blaauw & Christen, 2011; Figure 2).

Measurements of each u-channel were made at 1-cm resolution. NRM of each u-channel was stepwise demagnetized with three-axis alternating fields (AFs) at 5-mT increments for 0- to 50-mT peak fields, and at 10-mT increments for 60- to 100-mT peak fields. After AF treatments of each u-channel, anhysteretic remanent magnetization (ARM) was imparted in a direct current field of 0.05 mT and a maximum AF of 100 mT. ARM was demagnetized with the same AF steps used to demagnetize NRM. Both NRM and

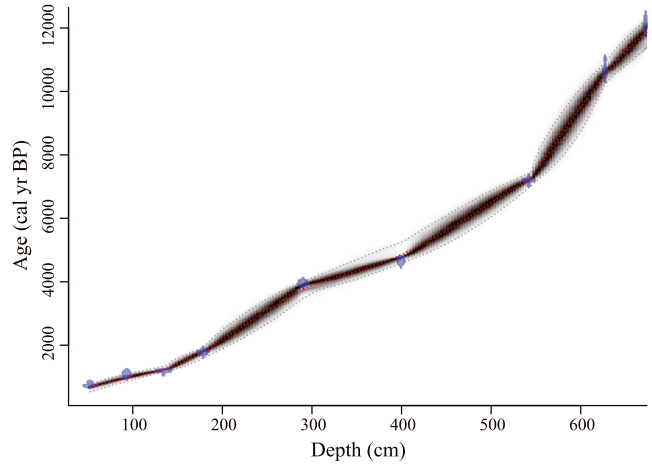

Figure 2. The age versus depth profile of the Huguangyan Maar Lake sediments constructed using the Bayesian age modeling tool Bacon 2.2 (Blaauw & Christen, 2011).

ARM measurements were conducted on a 2G-760 rock superconducting magnetometer in field-free room (<300 nT) at the Institute of Geology and Geophysics, Chinese Academy of Sciences (Beijing, China). The direction of characteristic remanent magnetization (ChRM) is calculated by principle component analysis (Kirschvink, 1980). An average of nine AF steps was used to define the ChRM with not-anchored fitting; the allowed maximum angle of deviation is set at 5°. The RPI record is generated by normalizing the NRM data by ARM, demagnetized at a common peak field in order to eliminate viscous remanence overprints. The $NRM_{25\ mT}/ARM_{25\ mT}$, $NRM_{30\ mT}/ARM_{30\ mT}$, $NRM_{35\ mT}/ARM_{35\ mT}$, $NRM_{40\ mT}/ARM_{40\ mT}$, $NRM_{45\ mT}/ARM_{45\ mT}$, and $NRM_{50\ mT}/ARM_{50\ mT}$ are averaged for the mean NRM/ARM. In addition, a total of 16 samples were selected from different depths of the composite core for measurements of magnetic hysteresis parameters by a MicroMag 3900 vibrating sample magnetometer in the Institute of Geophysics, China Earthquake Administration (Beijing, China). The hysteresis loops were autocorrected for the high-field contribution. First-order reversal curves (FORCs) were also measured for the same 16 samples with an averaging time of 0.1 s per data point and a field step of 1.84 mT.

Mineral magnetic parameters were determined for all discrete cube samples. Frequency-dependent magnetic susceptibility (χ_{fd}; in units of cubic meters per kilogram), a proxy for detecting the presence of very small, superparamagnetic particles (e.g., Evans & Heller, 2003; Liu et al., 2005), was determined using an AGICO MFK1-FA susceptometer at frequencies of 976, 3904, and 15616 Hz (with sensitivities of 2×10^{-8}, 6×10^{-8}, and 12×10^{-8} SI, respectively) in a peak magnetic field of 200 A/m. Here χ_{fd} is defined as $\chi_{976\ Hz} - \chi_{15,616\ Hz}$. Saturation isothermal remanent magnetization (SIRM) was induced in a direct current field of 1 T using an ASC Model IM-10-30 pulse magnetizer and measured using a 2G Enterprises Model 755-4K superconducting rock magnetometer. χ_{ARM} is the mass-normalized ARM (in ampere-square meters per kilogram) per unit bias field (H, in amperes per meter); its most useful property is that it preferentially responds to small single domain particles (Evans & Heller, 2003). χ_{ARM}/χ is adopted to indicate magnetic grain size (Oldfield, 1994; Thompson et al., 1980; Thompson & Oldfield, 1986). All magnetic parameters have been corrected for contributions from water content.

3. Results

3.1. Magnetic Mineralogy and Grain Size

All samples exhibit similar hysteresis behavior with a slightly wasp-waisted shape (Figure 3), indicating populations of grains with different coercivities. These loops generally close below 200 mT, indicating the dominance of low-coercivity ferrimagnetic minerals. The average B_c value ($n = 16$) is 8.1 mT, further suggesting the predominance of soft magnetic minerals. FORC diagrams of representative samples yield a central ridge on the B_c axis and a peak coercivity at about $B_c = 16$ mT (Figure 4), which are characteristic of weakly interacting single-domain magnetite (Roberts et al., 2000). The nearly vertical contours at the origin of the FORC diagram suggest that superparamagnetic particles are also significantly present.

3.2. Paleomagnetic Directions and "RPI"

The orthogonal demagnetization plots of nine representative samples from different depths in the composite core are shown in Figure 5. Nearly all samples demagnetized univectorially toward the origin which yielded well-defined paleomagnetic directions. For the majority of samples, a secondary magnetization is either absent (e.g., C4 bottom-18) or removed by AF demagnetization of 10 mT (e.g., B1 top-59). Quite a few continuous samples from the B1 bottom u-channel (e.g., B1 bottom-72 and B1 bottom-82) appear to be overprinted by a spurious magnetization (Figure 5), which is likely to be acquired during coring or u-channel preparation. The samples that recorded the notably low inclinations at ~60-cm and high inclinations at ~125-cm depths are also shown in Figure 5 (i.e., B1 top-77 and B1 bottom-35).

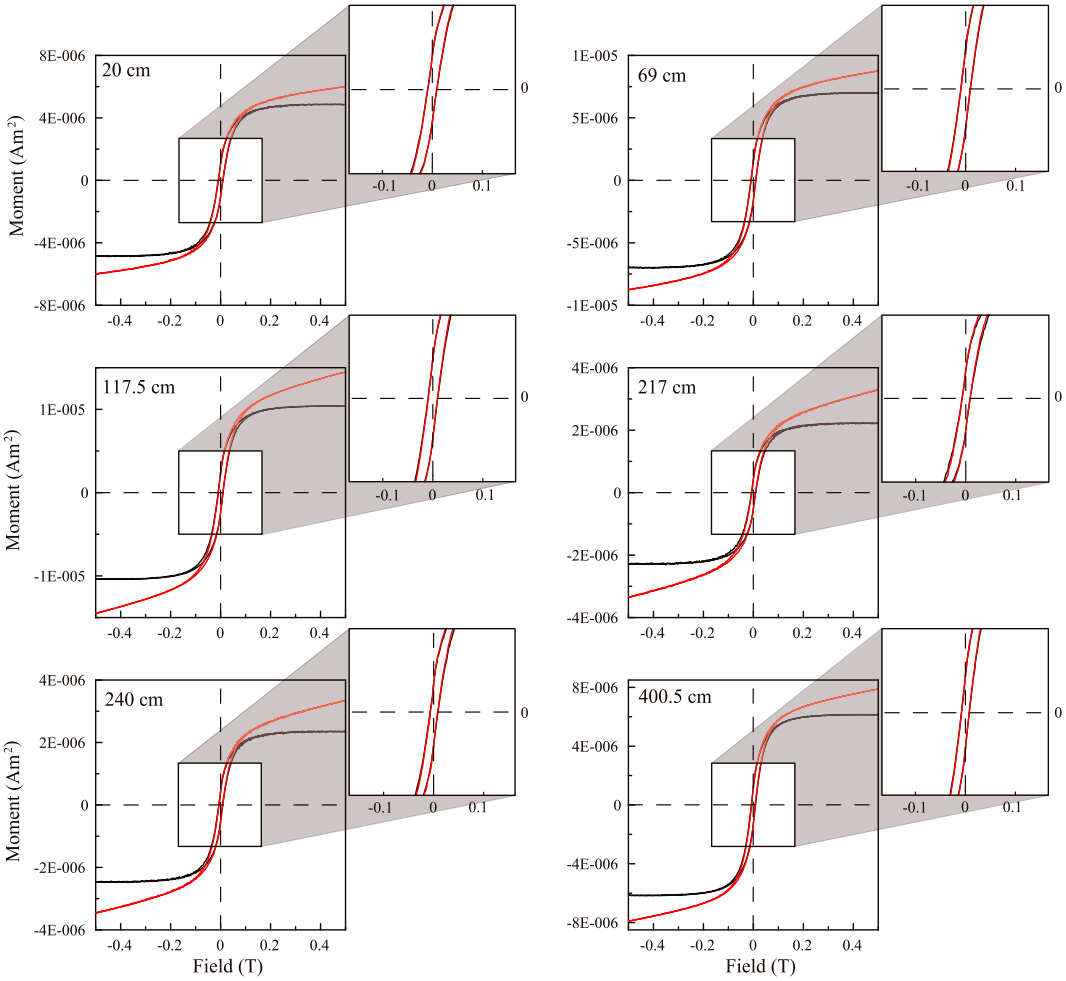

Figure 3. Hysteresis loops for representative samples. Red (black) loop is before (after) paramagnetic correction. The insets are enlargement of the central portions of the loops.

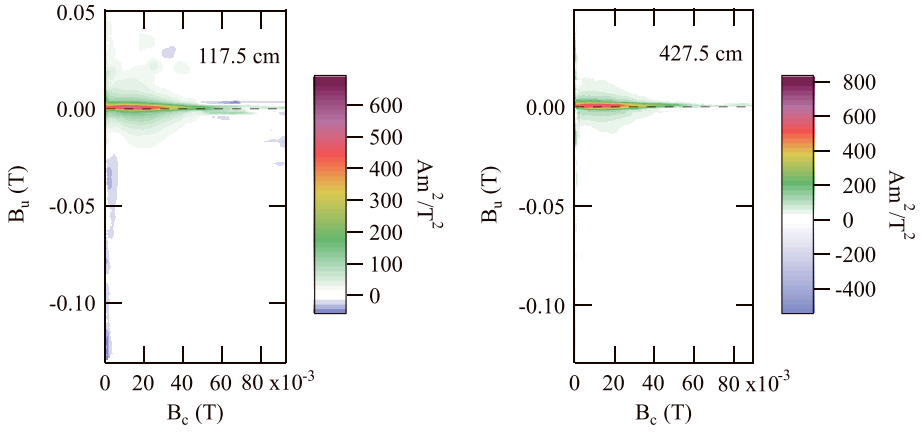

Figure 4. First-order reversal curve diagrams for representative samples from relatively weak (left) and strong (right) magnetic intervals. B_c is the coercive force. B_u corresponds to the distribution of interaction fields. Smoothing is performed using FORCinel 3.0 (Harrison et al., 2018) with parameters $S_{c0} = 4$, $S_{c1} = 7$, $S_{b0} = 3$, $S_{b1} = 7$, $\lambda_c = 0.1$, and $\lambda_c = 0.1$.

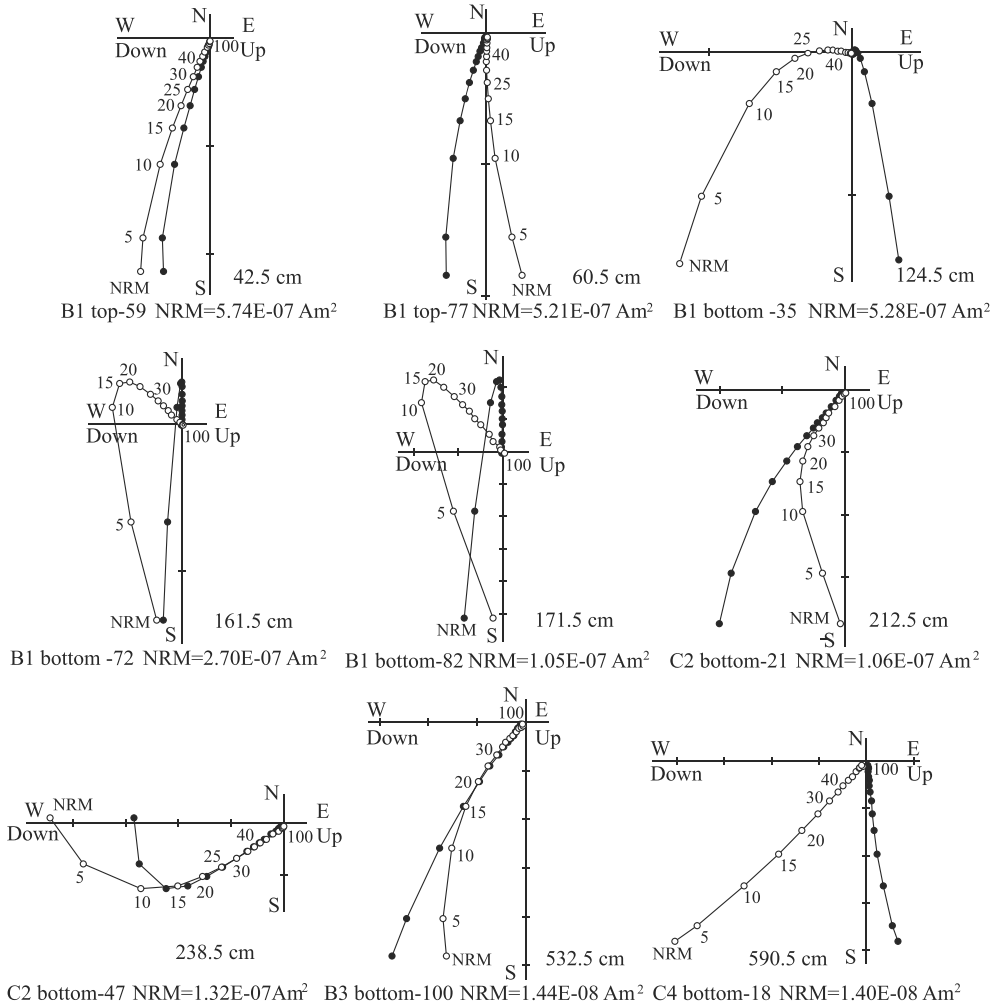

Figure 5. Orthogonal projection of natural remanent magnetization (NRM) vectors for selected Huguangyan Maar Lake samples after stepwise alternating field demagnetization. Solid circles plot on the horizontal plane and open circles on the vertical plane. Numbers on the diagrams are alternating field steps in milliteslas. The samples with the same prefix, for example, B1 up, are obtained from the same u-channel. The depth (centimeters below sediment water interface) and initial NRM intensity (Am^2) for each sample is given.

Because the core is not azimuthally oriented, the declination data were obtained by aligning the mean declination of each u-channel to the geographic north. Down-core variations of inclination, relative declination, $NRM_{25–50\ mT}$, $ARM_{25–50\ mT}$, RPI, SIRM, χ_{ARM}, and χ_{fd} are plotted in Figure 6. From the bottom to 240 cm of the composite core, inclinations vary from 14.4° to 64.8° with an average of 42.7° (Data Set S1). The upper 240 cm exhibits large-amplitude variations in inclination ranging from 0.6° to 82.8° with an average value of 35.9°. The mean inclination value over the entire Holocene is 40.4°, slightly steeper than the expected geocentric dipole inclination of ~37.7° at the HML area (red vertical line in Figure 6). Up-core variations are as follows. From bottom to 500 cm, AF demagnetization reveals that stable ChRMs, which are either slightly shallower or steeper than the expected geocentric dipole inclination, are clearly recorded. This implies that inclinations of this interval are not severely affected by environmental factors despite very low concentrations of ferrimagnetic minerals (Figure 7a). Inclinations between 500 and 240 cm are characterized by low-amplitude oscillations. From 240 to 128 cm, a distinct up-core increase is observed from an evident low of ~26.8° at the depth of ~240–200 cm to a significant high of 80° at the depth of ~110–128 cm. Between 128 and 70 cm, the inclinations exhibit a significant upward decrease and reach the shallowest level of ~0° at the depths of ~60–70 cm. From 60 to 40 cm, an up-core increase of inclination is observed. For the uppermost 40 cm, inclinations remain relatively stable. The relative declination exhibits a gradual westward drift from the bottom to 500 cm, followed by a marked eastward drift from 500 to 450 cm. The most easterly

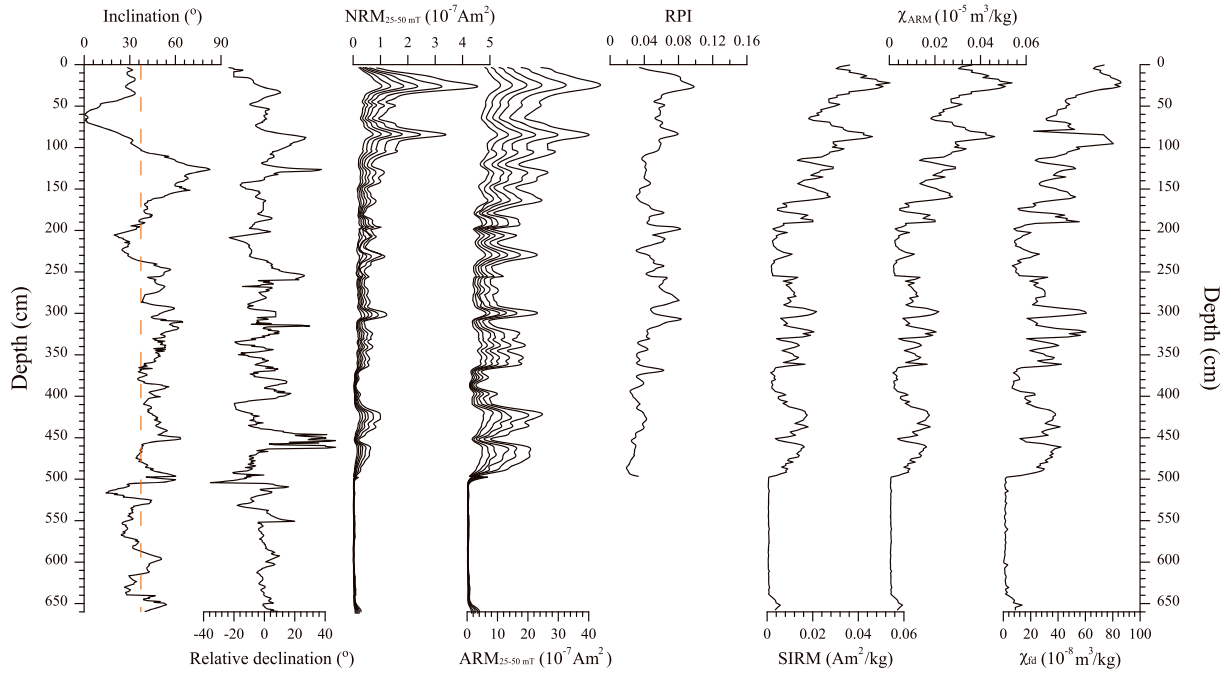

Figure 6. Variations in inclination, relative declination, $NRM_{25–50\ mT}$ (natural remanent magnetization), $ARM_{25–50\ mT}$ (anhysteretic remanent magnetization), relative paleointensity (RPI), SIRM (saturation isothermal remanent magnetization), χ_{ARM} (anhysteretic remanent susceptibility), and χ_{fd} (frequency-dependent susceptibility) with depth. Only the RPI variation for the upper 500 cm of the core is reconstructed because environmental factors precluded a meaningful determination at deeper levels (also the upper portion of the core appeared to be contaminated by variable diagenesis, see main text). The vertical red dashed line indicates the expected geocentric dipole inclination of ~37.7° at Huguangyan Maar Lake. The six curves in $NRM_{25–50\ mT}$ with depth from right to left are $NRM_{25\ mT}$, $NRM_{30\ mT}$, $NRM_{35\ mT}$, $NRM_{40\ mT}$, $NRM_{45\ mT}$, and $NRM_{50\ mT}$, respectively. The six curves in $ARM_{25–50\ mT}$ with depth from right to left are $ARM_{25\ mT}$, $ARM_{30\ mT}$, $ARM_{35\ mT}$, $ARM_{40\ mT}$, $ARM_{45\ mT}$, and $ARM_{50\ mT}$, respectively.

declination values (~40°) are observed at ~450 cm, which is followed upward by a westward movement from 450 to 410 cm. Between 410 and 250 cm, declinations show low-amplitude oscillations, with a westward deviation from 410 to 330 cm. Further up, it shows a gradual westward trend from 250 to 200 cm and a stepwise eastward trend from 200 to 100 cm. For the uppermost 100 cm, a stepwise westward trend is defined.

Both NRM and ARM are featured by extremely low value from the bottom to 500 cm in depth, followed by a sharp increase of 2 orders of magnitude from ~500 cm. A general upward increase from 500 cm to the top of

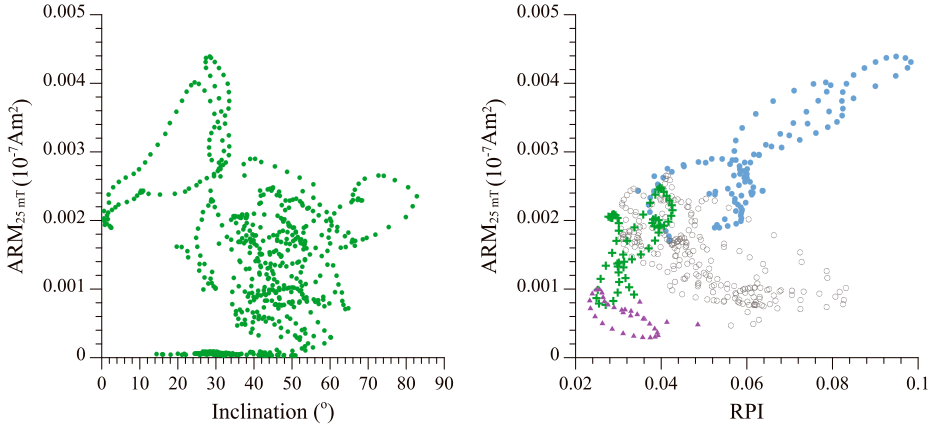

Figure 7. Biplots of (a) $ARM_{25\ mT}$ against inclination for the samples from the upper 670 cm of the core and (b) $ARM_{25\ mT}$ against RPI for the samples from the upper 500 cm. The solid blue circles, open circles, purple triangles, and green crosses in (b) represent samples from 0–120, 120–370, 370–410, and 410–500 cm, respectively. ARM = anhysteretic remanent magnetization; RPI = relative paleointensity.

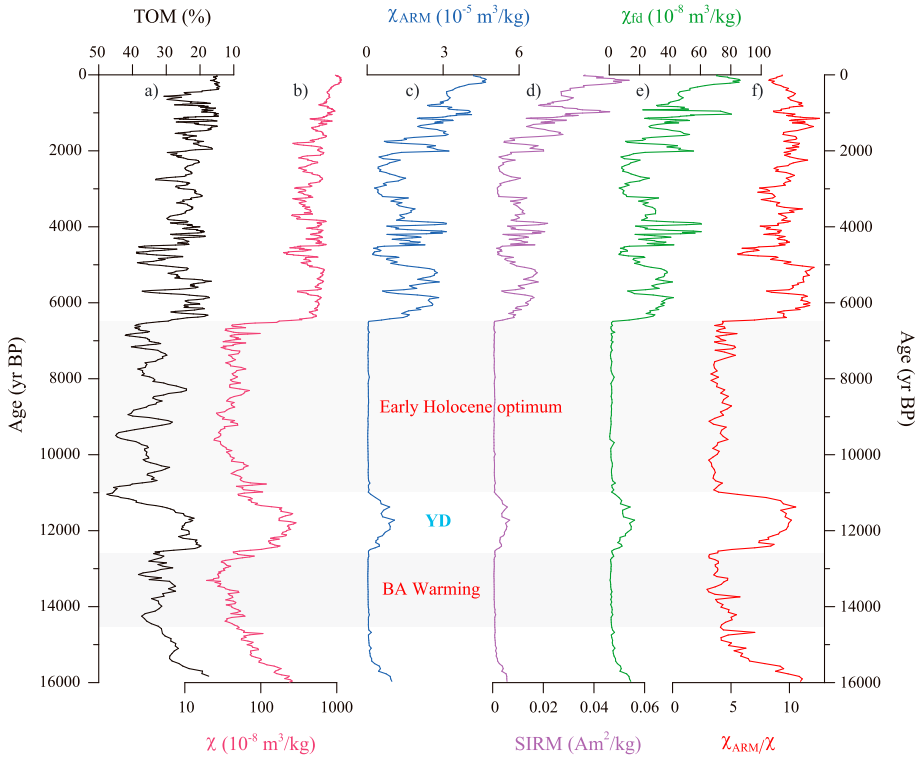

Figure 8. Comparison of magnetic parameters with the total organic matter (TOM) record over the past 16 kyr BP. This age range is chosen for optimal visualization of the coherence of TOM with magnetic parameters. (a) TOM. (b) χ on a logarithmic scale. (c) χ_{ARM}. (d) saturation isothermal remanent magnetization (SIRM). (e) χ_{fd}. (f) χ_{ARM}/χ. Note that TOM and χ data are reproduced from Wang et al. (2016). Two light gray bars indicate the timing of the Bølling-Allerød (BA) warming and early Holocene optimum, respectively. YD = Younger Dryas.

the core is observed (Figure 6). NRM, ARM, SIRM, χ_{fd}, and χ_{ARM} throughout the core show coherent variations (Figures 6 and 8). Higher (lower) NRM, χ_{ARM}, and SIRM values generally correspond to higher (lower) χ_{fd} and χ_{ARM}/χ, probably implying that more fine-grained ferrimagnetic minerals are present in the intervals of higher concentrations of ferrimagnetic minerals. Alternatively, if concentrations of ferrimagnetic minerals vary significantly throughout the core, χ_{fd} and χ_{ARM}/χ may be less suitable as proxies of magnetic grain size. It is generally accepted that the generation of reliable paleointensity requires magnetite mineralogy with relatively homogeneous concentration and grain sizes throughout the sequence (King et al., 1982; Tauxe, 1993). Therefore, an RPI record is only constructed for the upper 500 cm of the core, in which the concentration and grain size of magnetic minerals are relatively uniform; as we cannot rule out diagenetic impact entirely, the record is deemed tentative. The ARM variability covaries with that of NRM in the 25- to 50-mT demagnetization steps, indicating that the coercivity of ARM is a close match to that of NRM in this demagnetization range. Moreover, there is a slight increasing trend for the RPI upward the core from 500 cm. The RPI shows a positive correlation with ARM at the depths of 0–120 and 410–500 cm but a negative correlation at the depths of 120–370 and 370–410 cm, implying that the RPI is possibly affected by variations in mineral magnetic concentration and/or magnetic grain size (Figure 7b).

4. Discussion

4.1. Magnetic Mineralogy and Grain Size

Previous comparison of rare Earth element distribution patterns for samples from the HML sediments and surrounding volcanic rocks confirm that the HML sediments primarily originate from local pyroclastic rocks with strong magnetic signal (Wang et al., 2016). During and after sediment accumulation, the magnetic properties of sediments can be adversely affected by environmental factors (Tauxe, 1993). To extract reliable PSV and paleointensity estimates, it is important to investigate whether the NRM and RPI records show a

relationship with environmental parameters. The χ record exhibits a general trend of decreasing down core, implying a decrease of magnetic concentration. The total organic matter (TOM) content, which primarily reflects lake productivity as well as the contribution of terrestrial organic matter, is high during the early Holocene climatic optimum (approximately 11,500–6,500 years BP) and Bølling-Allerød warming period (approximately 15,000–13,000 years BP) and relatively low during middle-late Holocene (6,500 years BP to present) and the Younger Dryas cooling event (13,000–12,000 years BP; Wang et al., 2016; Figure 8). The generally low TOC/TN ratios of 7.0–12.5 throughout the Holocene suggest the down-core organic matter is predominantly of aquatic origin (Jia et al., 2015). The significant increase in total organic carbon, total sulfur, and sum of aquatic and wetland taxa in the magnetically depleted zones further suggests greater algal contributions and/or better preservation of organic matter in anoxic lake bottom as a result of a stagnant water column (Sheng et al., 2017; Wang et al., 2016; Wu et al., 2012; Yancheva et al., 2007). The inverse relationship between χ (magnetic concentration indicator) and TOM therefore implies that the HML magnetic record is evidently affected by organic matter diagenesis that causes dissolution of detrital iron-bearing minerals via iron reduction (Wang et al., 2016). In this study, more magnetic parameters, such as χ_{ARM}, SIRM, χ_{fd}, and χ_{ARM}/χ (Data Set S2), also show a negative correlation with TOM (Figure 8), indicating that the time intervals with low magnetic-mineral concentrations in an anoxic-sulfidic-dominated environment (Wang et al., 2016) may correspond to significant decreases in the proportion of fine-grained ferrimagnetic minerals and therefore "coarsening" of magnetic grain sizes. In contrast, the high magnetic-mineral concentrations intervals in a weakly reductive environment correspond to relatively fine magnetic particles. Previous studies also demonstrate that larger magnetic particles are present in periods with early diagenesis of organic matter in anoxic conditions (Jelinowska et al., 1997). The relationship between magnetic particle size and concentration-indicative magnetic parameters and TOM further demonstrates that the magnetic signal is largely affected by the redox processes in the lake, especially during the early Holocene climatic optimum and the Bølling-Allerød warming (Figure 8).

Fortunately, all of the orthogonal plots throughout the core exhibit a well-defined and stable ChRM after AF retreatments of 10–25 mT, which meets the requirement for a sedimentary sequence to record a reliable geomagnetic direction. No correlation between inclination and $ARM_{25\ mT}$ is observed (Figure 7a), implying that inclination fluctuations are insignificantly disturbed by the redox processes in the lake. Also, during the early Holocene climatic optimum with its significantly decreased magnetic concentrations because of the reductive dissolution of magnetic minerals, the partial preservation of detrital ferrimagnetic minerals and deposition-related remanent magnetization still means that genuine geomagnetic direction information may have been largely recorded.

However, retrieving a reliable paleointensity is a daunting task, especially for the periods with enhanced diagenetic alteration. The normalization of the NRM by ARM is expected to compensate for changes in concentration of remanence carrying grains down core (Tauxe, 1993). As shown in Figures 6 and 8b, RPI and environmental indicators (e.g., $ARM_{25\ mT}$) are positively correlated at the depth intervals of 0–120 cm (1,200 years BP to present) and 410–500 cm (6,000 to 4,800 years BP), implying the influence of mineral magnetic concentration. A negative correlation between RPI and $ARM_{25\ mT}$ at the depth of 120–410 cm (4,800–1,200 years BP) is observed, suggesting that the RPI record is affected by magnetic grain size as well. We therefore refrain from further discussion of the RPI implications since it is difficult to extract a meaningful RPI record from HML sediments even in the case of preservation of a strong magnetic signal.

4.2. PSV Comparison With Other Records From East Asia

To place the new Holocene HML PSV record into a regional context, we now compare it with other sediment records and also with archeological and volcanic data, all from East Asia (Figure 9). Archeological and volcanic PSV data from East Asia including China, Korea, Japan, and Thailand were downloaded from the GEOMAGIA50.v3 database (Brown et al., 2015); we also include the recently published data from Cai et al. (2016). Only those archeological and volcanic data with $\alpha_{95} \leq 10°$ and σ_{age} (age uncertainty) ≤ 500 years are included in Figure 9. All the archeological and volcanic inclinations have been relocated at the geographic coordinates of the HML location (21°9′N, 110°17′E) via the virtual geomagnetic pole method to exclude differences caused by different latitudes (Noël & Batt, 1990). Archeological material or lava flows can provide PSV data with high precision and high temporal resolution. The selected Holocene archeological

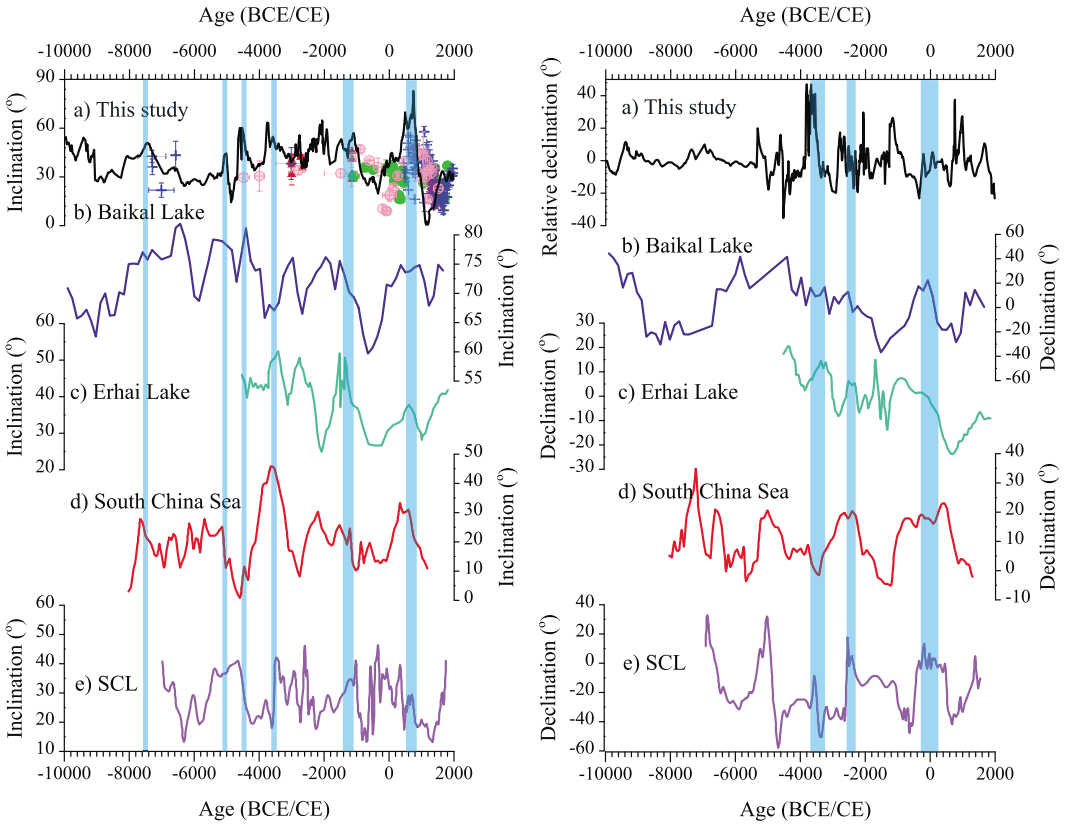

Figure 9. Comparison of Huguangyan Maar Lake (HML) inclination (left) and relative declination (right) with typical records from East Asia. (a) HML (this study), (b) Baikal Lake (Peck et al., 1996), (c) Erhai Lake (Hyodo et al., 1999), (d) South China Sea (Yang et al., 2016), and (e) Shuangchiling (SCL; Yang et al., 2009). Green circles, purple stars, blue plus signs, and pink circles are the archeological and volcanic data from Korea, Thailand, Japan, and China from the GEOMAGIA50 database after data selection (criteria in main text). Red triangles represent the published data from Cai et al. (2016). The archeological and volcanic data in this figure are relocated to the HML location (21°9′N, 110°17′E). The blue vertical bars represent the common paleomagnetic secular variation features between HML and other records from East Asia.

and volcanic data from China, Korea, Japan, and Thailand show good resemblance, within age uncertainty, with the HML inclinations, reinforcing the robustness of the HML inclination records.

Because the archeological and volcanic data are unevenly distributed and inherently discontinuous, we also compare our PSV with continuous and well-dated sediment records from East Asia, including Baikal Lake (55°N, 105°E) in Russia (Peck et al., 1996), Erhai Lake (25°50′N, 110°11′E; Hyodo et al., 1999), Shuangchiling (SCL) maar lake (19°56′N, 110°10′E; Yang et al., 2009), and northern South China Sea (19°03′N, 114°44′E; Yang et al., 2016) in southern China (also in Figure 9). The Baikal Lake PSV record comes from the Selenga prodelta region of and spans the last 84 kyr; its age model during the Holocene is constrained with six reliable AMS ^{14}C ages (Peck et al., 1996). Before the Holocene, that record shows a geomagnetic excursion at 20 ka and three large amplitude PSV swings at 41, 61, and 67 ka. During the Holocene, the HML inclination variation is synchronous and strongly correlative with the Baikal Lake record: inclination highs at ~7,500 BCE, ~6,700 BCE, ~5,100 BCE, ~4,600 BCE, ~1,600–1,200 BCE, and 600–800 CE and inclination lows at ~9,000 BCE, 300–600 BCE, and ~1,000–1,300 CE are observed in both records. The relative declination also shows similar features such as slightly eastward trends at ~4,600 BCE and 400 BCE to 200 CE. The PSV record from Erhai Lake since the last 6.5 ka, constrained by seven AMS ^{14}C ages, is fairly consistent with archaeomagnetic records from Luoyang in central China (Wei et al., 1981) and Japan (Hirooka, 1971; Maenaka, 1990) for the last 2 kyr, such as the inclination lows at 300–600 BCE and ~1,000–1,300 CE (Hyodo et al., 1999). Besides the above common characteristics, the PSV record from HML when compared with that from Erhai Lake also shows a similar inclination peak at ~3,600–3,400

BCE and an eastward trend at ~3,600–3,200 BCE, ~2,600–2,400 BCE, and 400 BCE to 200 CE. In addition, a PSV record based on 10 AMS ^{14}C ages from SCL reliably represents the Earth's magnetic field variations in South China for the last ~9,000 years (Yang et al., 2009). The HML Holocene inclination shows a similar behavior with that of SCL especially at ~6,700 BCE, 4,000 BCE, 3,600–3,400 BCE, ~1,600–1,200 BCE, and 600–800 CE. The HML relative declination behavior is consistent with the eastward trends at ~2,600–2,400 BCE and 400 BCE to 200 CE in SCL. The more recent Holocene PSV record, based on nine AMS ^{14}C dates from the northern South China Sea (Yang et al., 2016), is quite consistent with the SCL record. The PSV records of HML and the South China Sea are also highly comparable; both records show seven inclination highs at ~7,500 BCE, ~6,700 BCE, ~5,100 BCE, ~3,600–3,400 BCE, ~2,200 BCE, ~1,600–1,200 BCE, and 600–800 CE; four inclination lows at ~4,800 BCE, ~2,800 BCE, 300–600 BCE, and ~1,000–1,300 CE; and eastward (relative) trends at ~5,400–5,000 BCE, ~2,600–2,400 BCE, and 400 BCE to 200 CE. Overall, the regional similarities in both inclination and declination especially with SCL, which is most nearby to HML, corroborate the validity both of our revisited age model and the PSV record. Even though the HML inclination high at ~600–800 CE up to 80° and inclination low at ~1,000–1,300 CE approaching the equator could be of larger amplitude than the real PSV because of probable physical distortion during the coring, we still believe that they may reflect geomagnetic behavior. Our PSV record provides a regionally important PSV reference curve, whose conspicuous features including six inclination highs at ~7,500 BCE, ~5,100 BCE, ~4,600 BCE, ~3,600–3,400 BCE, ~2,200–1,200 BCE, and ~600–800 CE; four inclination lows at ~9,000 BCE, ~4,800 BCE, ~300–600 BCE, and ~1,000–1,300 CE; and six distinctly eastward declination trends at ~4,600 BCE, 3,600–3,200 BCE, ~2,600–2,400 BCE, and 400 BCE to 200 CE may be considered as stratigraphic markers for East Asian records.

We should note that all recent magnetic studies of HML unanimously reveal a dramatic rise in magnetic signal that represents a major environmental degradation during the early-middle Holocene transition (Duan et al., 2014; Jia et al., 2015; Sheng et al., 2017; Wang et al., 2016; Wu et al., 2012, 2016; Yancheva et al., 2007). In our study, this major climatic event commences at the depth of ~498 cm with a calibrated ^{14}C age of ~6.4 ka BP. This age is nearly identical to that of ~6.3 ka BP as reported by Wu et al. (2012), whose age model was precisely constrained by 18 reliable AMS ^{14}C dating during the Holocene. The earlier PSV study by Yang et al. (2012) has also clearly defined this prominent magnetic increase at the depth of 320 cm with a calibrated ^{14}C age of ~6.4 ka BP. Considering possible lock-in and/or old carbon effects, however, they revised their AMS ^{14}C-based age model by visually correlating their PSV record with those from North Hemisphere, yielding a significantly younger age of ~5.5 ka BP for this abrupt climate shift. This arbitrary shift results in a marked age discrepancy of 1,000 years with recent studies from HML throughout the Holocene (e.g., Jia et al., 2015; Wang et al., 2016; Wu et al., 2012). More specifically, their inclination results are generally 10° shallower than the expected geocentric dipole inclination in HML area and the degree of shallowing increases with depth, which points to effects of compaction (Yang et al., 2012). In particular, their cores were retrieved from SW margin of the lake, where the lake floor is almost steepest, as revealed by previous bathymetric measurements (Yancheva et al., 2007). The sedimentary sequence with great water-depth gradient is prone to be controlled by very local sedimentary conditions and is therefore not an ideal position for drilling. In addition, the average sedimentation rate of our core ranges from 33 cm/kyr during 10,000–4,500 BCE to 112 cm/kyr since 4,500 BCE, which is evidently higher than that of Yang et al. (2012; 26.5–59.3 cm/kyr). Our core site with a higher-sediment accumulation rate and much flatter lake floor is more suitable for coring. Also, our higher sampling resolution and better age constraints enable us to obtain a well-dated and more accurate PSV record, which is valuable for stratigraphic correlation and dating on regional scale.

4.3. Comparison With Records From the Northern Hemisphere

In order to assess the spatial extent of PSV features, robust records from the Northern Hemisphere including Lake Kalksjon in Sweden (Stanton et al., 2010; Stanton et al., 2011), Lake Nautajarvi in Finland (Ojala & Tiljander, 2003), the U.K. master curve (Turner & Thompson, 1981), the Demerara Rise in the equatorial west Atlantic Ocean (Lund et al., 2017), the Eastern U.S. stack (King & Peck, 2001), and the Eastern Canada stack (Barletta et al., 2010) are also displayed (Figure 10). Although each record comes with uncertainties in its age model, several notable magnetic inclination and declination features on centennial to millennial scale can be correlated over the various records. For instance, a trough (with number 1 in Figure 10) at ~1,000–1,300 CE and six peaks, numbered 2–7 in Figure 10, at ~9,700–9,500 BCE, 7,600–7,500 BCE, 4,700–

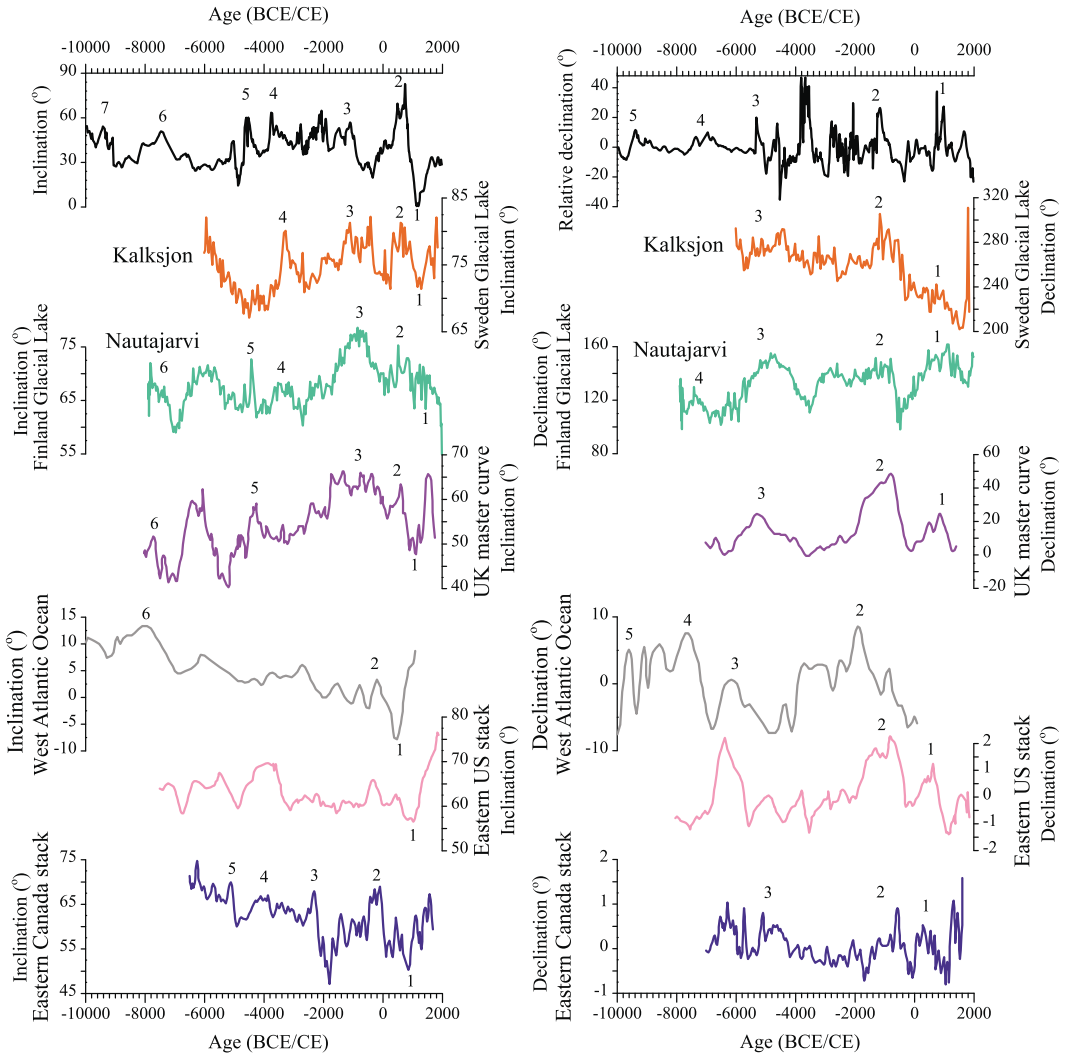

Figure 10. Comparison of Huguangyan Maar Lake inclination (left) and relative declination (right) with other records from the Northern Hemisphere. The black, red, green, purple, gray, pink, and dark blue lines represent the directional record from this study, Sweden (Stanton et al., 2010; Stanton et al., 2011), Finland (Ojala & Tiljander, 2003), U.K. master curve (Turner & Thompson, 1981), west Atlantic Ocean (Lund et al., 2017), eastern U.S. stack (King & Peck, 2001), and eastern Canada stack (Barletta, St-Onge, Stoner, et al., 2010), respectively.

4,500 BCE, 3,700–3,500 BCE, 1,400–1,200 BCE, and 400–800 CE from the HML inclination record are also recognized in other records from Northern Hemisphere (within allowable age uncertainties). In the (relative) declination records, five eastward trends at ~9,700–9,500 BCE, 7,600–7,400 BCE, 5,400–5,200 BCE, 1,400–1,200 BCE, and 600–800 CE are also documented in the HML and other Northern Hemisphere records. These levels can thus be used as key regional stratigraphic markers. Perceived age differences may be caused by the contamination of "old carbon" in lacustrine sediment as was demonstrated in the eastern U.S. stack records (King & Peck, 2001) and the U.K. master curve (Turner & Thompson, 1981), or possible lock-in related processes.

The comparison of Holocene PSV records from eight North American lakes indicates that some aspects of the geomagnetic field behave coherently over roughly a continental scale (Lund, 1996). Comparisons of inclination and declination features from eastern Canada with North American Holocene PSV records are generally consistent and temporal offsets are within chronological uncertainties (St-Onge et al., 2003). By comparing the PSV of eastern Canadian stack with other records, Barletta, St-Onge, Stoner, et al. (2010) noted that the PSV spatial scale can be further extended beyond the North American continent to Iceland

and Europe, suggesting a common, geomagnetic origin, possibly hemispheric in character. Also, the HML record, along with other East Asian records, further suggests that such directional patterns could indeed be hemispheric in scale.

PSV can provide a powerful probe of the dynamics of the top of the Earth's core and ultimately of the whole geodynamo (Korte & Holme, 2010). Historically persistent regions of concentrated geomagnetic flux (i.e., flux lobes) at the core-mantle boundary are detected at high-latitude locations in the Northern Hemisphere below Canada, Siberia, and Europe (e.g., Bloxham & Gubbins, 1985; Gubbins & Bloxham, 1987). High-resolution PSV reconstructions show that magnetic field pattern can be roughly divided into two modes consistent with a geomagnetic flux lobe over North America alternating in dominance with a flux lobe over Europe (Gallet et al., 2009; Stoner et al., 2013). The Holocene PSV may largely result from time varying flux concentrations oscillating between a few recurrent high-latitude locations (Stoner et al., 2013). As observed in Figure 10, both the inclination and relative declination from HML in East Asia correlate better with European than with North American and Canadian records. This may be attributed to the flux lobe competition between the sites of East Asia and the North American and European reginal records (Avery et al., 2017), with a weakening of the North American flux lobe and a strengthening of the Siberian-European flux lobes.

4.4. Comparison With Model Predictions

For the comparison between HML data and geomagnetic field models, we calculated the site's (21°9′N, 110°17′E) model inclination and declination for three short-term models covering the past 3 kyr: CALS3k.4 (Korte & Constable, 2011), ARCH3k.1 (Korte et al., 2009), and SED3k.1 (Korte et al., 2009). We did the same for four long-term models for the entire Holocene: CALS10k.1b (Korte et al., 2011), pfm9k.1a (Nilsson et al., 2014), CALS10k.2 (Constable et al., 2016), and HFM.OL1.AL1 (Constable et al., 2016; Panovska et al., 2015). The ARCH3k.1 and SED3k.1 models are constructed based on archeomagnetic and sediment data covering the past 3 kyr, respectively, while CALS3k.4 uses a combination of these two types of databases. CALS10k.1b covers the past 10 kyr and incorporates the largest number of data to date. CALS10K.2 incorporates nearly the same sediment data as CALS10k.1b and an updated set of lava and archeological data. CALS10k.2 is of higher temporal and spatial resolution than CALS10k.1b due to improved data uncertainty estimates for the sediment records. HFM.OL1.A1 covers the same time span and incorporates the same data as CALS10k.2 and has somewhat higher temporal but somewhat lower spatial resolution than CALS10k.2. The pfm9k.1a model spans the past 9,000 years and uses the same data set as CALS10k.1b but introduces new data processing approaches, particularly for the sedimentary data. These include redistributing the weight given to different data types and data sources, iteratively recalibrating relative declination data and adjusting the timescales of the sediment records using a preliminary model. Such data processing, particularly the timescale adjustments, reduces inconsistencies in the database and enables pfm9k.1a to capture larger amplitude PSV variations than the other models.

Typically, inclinations derived from CALS10k.2, HFM.OL1.A1, and pfm9k.1a are steeper than CALS10K.1b, which is closest to the HML record (Figure 11). For 8,000–7,000 BCE, the inclinations from HML show a striking resemblance with the CALS10K.1b model within age uncertainty, whereas they are slightly higher than CALS10K.2 and HFM.OL1. For the period of 7,000–4,500 BCE, the inclinations fit very well with CALS10K.2, HFM.OL1.A1, and pfm9k.1a, while they are slightly lower than CALS10K.1b. During 4,500–1,000 BCE, the inclinations from HML are in excellent agreement with the prediction of CALS10K.1b; they are generally higher than the predictions of the CALS10K.2, HFM.OL1.A1, and pfm9k.1a models. Specifically, even though pfm9k.1a predicts the observed peak inclinations around 4,500–4,400 BCE and 3,700–3,500 BCE, the model predictions are lower than those obtained in the HML record, which could be due to model smoothing. During the interval of 1,000–400 BCE, it seems that CALS10k.2, HFM.OL1.A1, pfm9k.1a, and ARCH3k.1 predictions better agree with HML inclinations than that of CALS10K.1b, CALS3k.4, and SED3k.1. During 400 BCE to 400 CE, HML inclinations are among CALS10K.1b, CALS3k.4, and SED3k.1 but distinctly higher than ARCH3k.1 and slightly higher than CALS10k.2, HFM.OL1.A1, and pfm9k.1a. Although all the models capture the cusp around 400–800 CE, which may correspond to one of the archeomagnetic jerks evidenced by Gallet et al. (2003), the HML inclinations are distinctly higher than the model predictions, which may be attributed to the

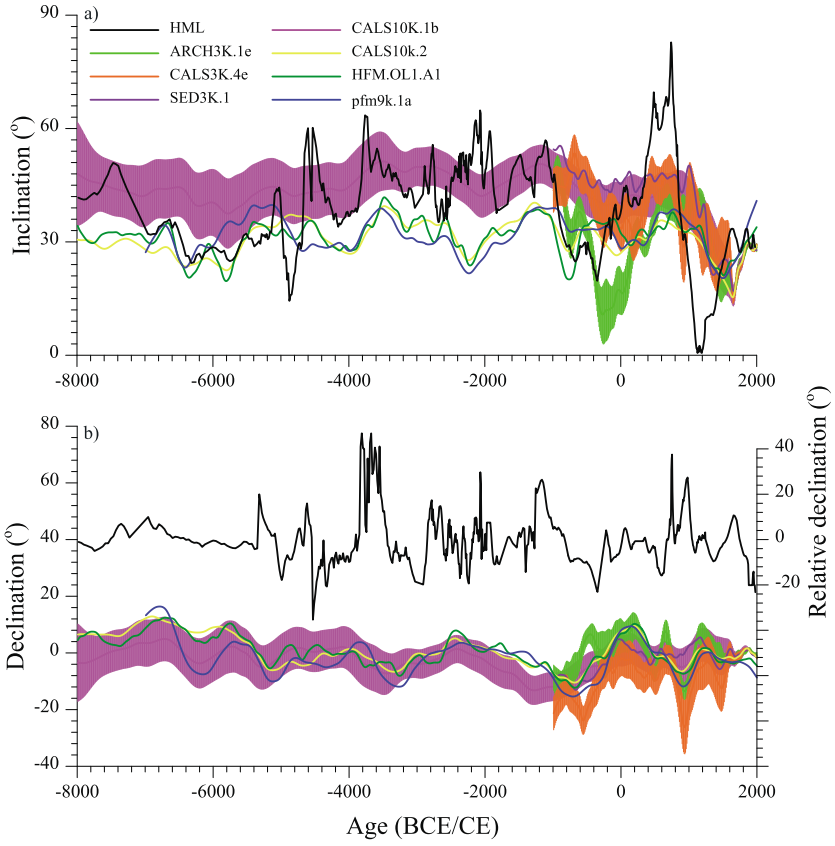

Figure 11. Comparison Huguangyan Maar Lake (HML) inclination (a) and relative declination (b) records with the global field models ARCH3k.1, CALS3k.4, SED3k.1, CALS10k.1b, CALS10k.2, HFM.OL1.AL1, and pfm9k.1a calculated at the HML location.

predictions being smoothed to a certain degree or/and to potential (small) drilling perturbations, for example, the mechanical deformation of the sediments during the piston coring. From 800–1000 CE, the HML inclination shows a rapid decrease, which confirm the prediction by the CALS3k.4 model. There is a notable inclination low during 1,000–1,300 CE, which is predicted by none of these models. However, deemed robust sediment records from South China such as SCL (Yang et al., 2009) and the northern South China Sea (Yang et al., 2016) and quite a few archeological and volcanic data from Japan also document this inclination low (Figure 9). Moreover, other records from the Northern Hemisphere, such as Lake Kalksjon in Sweden (Stanton et al., 2010; Stanton et al., 2011), the U.K. master curve (Turner & Thompson, 1981), and the Eastern U.S. stack (King & Peck, 2001), define an inclination low during 1,000–1,300 CE as well (Figure 10). Thus, we propose that it is likely to represent a genuine geomagnetic behavior although more reliable PSV records with robust age controls from East Asia are necessary to improve the global models during this period. Since 1300 CE, the measured average inclination fits well with all the predictions. In Figure 11b, there is good consistency between the HML relative declination and the long-term models during the Holocene. The three eastward trends at 7,100–6,600 BCE, 2,500–2,000 BCE, and 200 BCE to 200 CE, and two distinct westward trends at 500–300 BCE and 1,400–1,500 CE, predicted by pfm9k.1a, CALS10K.1b, CALS10K.2 and HFM.OL1, CALS3k.4, and SED3k.1, are comparable with the HML relative declination pattern within age uncertainty. In general, the directional information from South China during the Holocene seems best predicted by the CALS10K.1b and CALS3k.4 models, both of which are based on sediment data and supplemented by a set of lava and archeological data. All in all, the similarities between the HML PSV record and geomagnetic field models demonstrate that the HML PSV record, with more details than the models can deliver, represents genuine directional variations of the Earth's magnetic field in South China during the Holocene.

5. Conclusions

We obtained a high-resolution Holocene PSV record from HML in South China. Six distinct inclination peaks at ~7,500 BCE, ~5,100 BCE, ~4,600 BCE, ~3,600–3,400 BCE, ~1,600–1,200 BCE, and 600–800 CE and three inclination lows at ~4,800 BCE, ~600–300 BCE, and ~1,000–1,300 CE are recognized. This PSV record exhibits overall comparability with other records from East Asia with independent chronologies, collaborating the robustness of our age model. Centennial- to millennial-scale PSV features of the HML record can be well correlated, within some age uncertainties, with other Holocene European, American, and Canadian stacked PSV records, suggesting that such PSV patterns are likely hemispheric in scale. A rather good consistency is also observed between the HML PSV record and geomagnetic field models, supporting our arguments that this revisited PSV record may be regarded as a reliable PSV reference curve and therefore a valuable tool for regional stratigraphic correlation and dating purpose in South China.

Acknowledgments
This study was supported by the NSFC (Grants 41274074 and 41371219) and China Geological Survey (Grant DD20160306). The 1-year stay of Mei Sheng at Fort Hoofddijk was funded by the China Scholarship Council. We sincerely thank L. V. de Groot, W. Krijgsman, and C. Langereis for their constructive suggestions. Comprehensive reviews by Huapei Wang, one anonymous reviewer, and the Editor J. Feinberg are greatly appreciated. We are also grateful to Y. L. Su, Z. Y. Gu, and Q. Z. Zhu for their help during the coring campaign and in the laboratory. Data to support the main findings of this article are available in the supporting information.

References

Avery, R. S., Xuan, C., Kemp, A. E. S., Bull, J. M., Cotterill, C. J., Fielding, J. J., et al. (2017). A new Holocene record of geomagnetic secular variation from Windermere, UK. *Earth and Planetary Science Letters*, *477*, 108–122. https://doi.org/10.1016/j.epsl.2017.08.025

Barletta, F., St-Onge, G., Channell, J. E. T., & Rochon, A. (2010). Dating of Holocene western Canadian Arctic sediments by matching paleomagnetic secular variation to a geomagnetic field model. *Quaternary Science Reviews*, *29*(17-18), 2315–2324. https://doi.org/10.1016/j.quascirev.2010.05.035

Barletta, F., St-Onge, G., Stoner, J. S., Lajeunesse, P., & Locat, J. (2010). A high-resolution Holocene paleomagnetic secular variation and relative paleointensity stack from eastern Canada. *Earth and Planetary Science Letters*, *298*(1-2), 162–174. https://doi.org/10.1016/j.epsl.2010.07.038

Ben-Yosef, E., Millman, M., Shaar, R., Tauxe, L., & Lipschits, O. (2017). Six centuries of geomagnetic intensity variations recorded by royal Judean stamped jar handles. *Proceedings of the National Academy of Sciences of the United States of America*, *114*(9), 2160–2165. https://doi.org/10.1073/pnas.1615797114

Ben-Yosef, E., Tauxe, L., Ron, H., Agnon, A., Avner, U., Najjar, M., & Levy, T. E. (2008). A new approach for geomagnetic archaeointensity research: Insights on ancient metallurgy in the Southern Levant. *Journal of Archaeological Science*, *35*(11), 2863–2879. https://doi.org/10.1016/j.jas.2008.05.016

Blaauw, M., & Christen, A. (2011). Flexible paleoclimate age-depth models using an autoregressive gamma process. *Bayesian Analysis*, *6*(3), 457–474. https://doi.org/10.1214/11-BA618

Bloxham, J., & Gubbins, D. (1985). The secular variation of Earth's magnetic field. *Nature*, *317*(6040), 777–781. https://doi.org/10.1038/317777a0

Brown, M. C., Donadini, F., Korte, M., Nilsson, A., Korhonen, K., Lodge, A., et al. (2015). GEOMAGIA50.v3: 1. General structure and modifications to the archeological and volcanic database. *Earth, Planets and Space*, *67*(1). https://doi.org/10.1186/s4062

Cai, S., Chen, W., Tauxe, L., Deng, C., Qin, H., Pan, Y., et al. (2015). New constraints on the variation of the geomagnetic field during the late Neolithic period: Archaeointensity results from Sichuan, southwestern China. *Journal of Geophysical Research: Solid Earth*, *120*, 2056–2069. https://doi.org/10.1002/2014JB011618

Cai, S., Jin, G., Tauxe, L., Deng, C., Qin, H., Pan, Y., & Zhu, R. (2017). Archaeointensity results spanning the past 6 kiloyears from eastern China and implications for extreme behaviors of the geomagnetic field. *Proceedings of the National Academy of Sciences of the United States of America*, *114*(1), 39–44. https://doi.org/10.1073/pnas.1616976114

Cai, S., Tauxe, L., Deng, C., Pan, Y., Jin, G., Zheng, J., et al. (2014). Geomagnetic intensity variations for the past 8 kyr: New archaeointensity results from Eastern China. *Earth and Planetary Science Letters*, *392*, 217–229. https://doi.org/10.1016/j.epsl.2014.02.030

Cai, S., Tauxe, L., Deng, C., Qin, H., Pan, Y., Jin, G., et al. (2016). New archaeomagnetic direction results from China and their constraints on palaeosecular variation of the geomagnetic field in Eastern Asia. *Geophysical Journal International*, *207*(2), 1332–1342. https://doi.org/10.1093/gji/ggw351

Constable, C., Korte, M., & Panovska, S. (2016). Persistent high paleosecular variation activity in southern hemisphere for at least 10 000 years. *Earth and Planetary Science Letters*, *453*, 78–86. https://doi.org/10.1016/j.epsl.2016.08.015

Donadini, F., Korhonen, K., Riisager, P., & Pesonen, L. (2006). Database for Holocene geomagnetic intensity information. *Eos, Transactions American Geophysical Union*, *87*(14), 137. https://doi.org/10.1029/2006EO140002

Duan, Z., Liu, Q., Yang, X., Gao, X., & Su, Y. (2014). Magnetism of the Huguangyan Maar Lake sediments, Southeast China and its paleoenvironmental implications. *Palaeogeography, Palaeoclimatology, Palaeoecology*, *395*, 158–167. https://doi.org/10.1016/j.palaeo.2013.12.033

Ertepinar, P., Langereis, C. G., Biggin, A. J., Frangipane, M., Matney, T., Ökse, T., & Engin, A. (2012). Archaeomagnetic study of five mounds from Upper Mesopotamia between 2500 and 700 BCE: Further evidence for an extremely strong geomagnetic field ca. 3000 years ago. *Earth and Planetary Science Letters*, *357-358*, 84–98. https://doi.org/10.1016/j.epsl.2012.08.039

Evans, M. E., & Heller, F. (2003). *Environmental magnetism: Principles and applications of enviromagnetics*. San Diego, CA: Academic Press.

Gallet, Y., Genevey, A., & Courtillot, V. (2003). On the possible occurrence of 'archaeomagnetic jerks' in the geomagnetic field over the past three millennia. *Earth and Planetary Science Letters*, *214*(1-2), 237–242. https://doi.org/10.1016/S0012-821X(03)00362-5

Gallet, Y., Hulot, G., Chulliat, A., & Genevey, A. (2009). Geomagnetic field hemispheric asymmetry and archeomagnetic jerks. *Earth and Planetary Science Letters*, *284*(1-2), 179–186. https://doi.org/10.1016/j.epsl.2009.04.028

Gonzalez, S., Sherwood, G., Böhnel, H., & Schnepp, E. (1997). Palaeosecular variation in Central Mexico over the last 30000 years: The record from lavas. *Geophysical Journal International*, *130*(1), 201–219. https://doi.org/10.1111/j.1365-246X.1997.tb00999.x

de Groot, L. V., Béguin, A., Kosters, M. E., van Rijsingen, E. M., Struijk, E. L. M., Biggin, A. J., et al. (2015). High paleointensities for the Canary Islands constrain the Levant geomagnetic high. *Earth and Planetary Science Letters*, *419*, 154–167. https://doi.org/10.1016/j.epsl.2015.03.020

de Groot, L. V., Biggin, A. J., Dekkers, M. J., Langereis, C. G., & Herrero-Bervera, E. (2013). Rapid regional perturbations to the recent global geomagnetic decay revealed by a new Hawaiian record. *Nature Communications*, *4*(1), 2727. https://doi.org/10.1038/ncomms3727

Gubbins, D., & Bloxham, J. (1987). Morphology of the geomagnetic field and implication for the geodynamo. *Nature*, *325*(6104), 509–511. https://doi.org/10.1038/325509a0

Harrison, R. J., Muraszko, J., Heslop, D., Lascu, I., Muxworthy, A. R., & Roberts, A. P. (2018). An improved algorithm for unmixing first-order reversal curve diagrams using principal component analysis. *Geochemistry, Geophysics, Geosystems*, *19*, 1595–1610. https://doi.org/10.1029/2018GC007511

Hirooka, K. (1971). Archaeomagnetic study for the past 2000 years in southwest Japan. *Memoirs of the Faculty of Science, Kyoto University*, *38*, 167–207.

Hyodo, M., Yoshihara, A., Kashiwaya, K., Okimura, T., Masuzawa, T., Nomura, R., et al. (1999). A Late Holocene geomagnetic secular variation record from Erhai Lake, Southwest China. *Geophysical Journal International*, *136*(3), 784–790. https://doi.org/10.1046/j.1365-246x.1999.00764.x

Jelinowska, A., Tucholka, P., & Wieckowski, K. (1997). Magnetic properties of sediments in a Polish lake: Evidence of a relation between the rock-magnetic record and environmental changes in Late Pleistocene and Holocene sediments. *Geophysical Journal International*, *129*(3), 727–736. https://doi.org/10.1111/j.1365-246X.1997.tb04508.x

Jia, G. D., Bai, Y., Yang, X. Q., Xie, L. H., Wei, G. J., Ouyang, T. P., et al. (2015). Biogeochemical evidence of Holocene East Asian summer and winter monsoon variability from a tropical maar lake in southern China. *Quaternary Science Reviews*, *111*, 51–61. https://doi.org/10.1016/j.quascirev.2015.01.002

Kanamatsu, T., Usami, K., McHugh, C. M. G., & Ikehara, K. (2017). High-resolution chronology of sediment below CCD based on Holocene paleomagnetic secular variations in the Tohoku-oki earthquake rupture zone. *Geochemistry, Geophysics, Geosystems*, *18*, 2990–3002. https://doi.org/10.1002/2017GC006878

King, J., Banerjee, S. K., Marvin, J., & Ozdemir, O. (1982). A comparison of different magnetic methods for determining the relative grain size of magnetite in natural materials: Some results from lake sediments. *Earth and Planetary Science Letters*, *59*, 404–419. https://doi.org/10.1016/0012-821X(82)90142-X

King, J., & Peck, J. (2001). Use of paleomagnetism in studies of lake sediments. In W. M. Last, & J. P. Smol (Eds.), *Tracking environmental change using lake sediments. Volume 1: Basin analysis, coring, and chronological techniques* (pp. 371–389). Dordrecht, The Netherlands: Kluwer Academic Publishers.

Kirschvink, J. L. (1980). The least-squares line and plane and the analysis of palaeomagnetic data. *Geophysical Journal International*, *62*(3), 699–718. https://doi.org/10.1111/j.1365-246X.1980.tb02601.x

Kissel, C., Laj, C., Rodriguez-Gonzalez, A., Perez-Torrado, F., Carracedo, J. C., & Wandres, C. (2015). Holocene geomagnetic field intensity variations: Contribution from the low latitude Canary Islands site. *Earth and Planetary Science Letters*, *430*, 178–190. https://doi.org/10.1016/j.epsl.2015.08.005

Korhonen, K., Donadini, F., Riisager, P., & Pesonen, L. (2008). GEOMAGIA50: An archeointensity database with PHP and MySQL. *Geochemistry, Geophysics, Geosystems*, *9*, Q04029. https://doi.org/10.1029/2007GC001893

Korte, M., & Constable, C. (2005). Continuous geomagnetic field models for the past 7 millennia: 2. CALS7K. *Geochemistry, Geophysics, Geosystems*, *6*, Q02H16. https://doi.org/10.1029/2004GC000801

Korte, M., & Constable, C. (2011). Improving geomagnetic field reconstructions for 0–3 ka. *Physics of the Earth and Planetary Interiors*, *188*(3-4), 247–259. https://doi.org/10.1016/j.pepi.2011.06.017

Korte, M., Constable, C., Donadini, F., & Holme, R. (2011). Reconstructing the Holocene geomagnetic field. *Earth and Planetary Science Letters*, *312*(3-4), 497–505. https://doi.org/10.1016/j.epsl.2011.10.031

Korte, M., Donadini, F., & Constable, C. (2009). Geomagnetic field for 0-3 ka: 2. A new series of time-varying global models. *Geochemistry, Geophysics, Geosystems*, *10*, Q06008. https://doi.org/10.1029/2008GC002297

Korte, M., & Holme, R. (2010). On the persistence of geomagnetic flux lobes in global Holocene field models. *Physics of the Earth and Planetary Interiors*, *182*(3-4), 179–186. https://doi.org/10.1016/j.pepi.2010.08.006

Liu, Q., Torrent, J., Maher, B. A., Yu, Y., Deng, C., Zhu, R., & Zhao, X. (2005). Quantifying grain size distribution of pedogenic magnetic particles in Chinese loess and its significance for pedogenesis. *Journal of Geophysical Research*, *110*, B11102. https://doi.org/10.1029/2005JB003726

Lougheed, B. C., Nilsson, A., Björck, S., Snowball, I., & Muscheler, R. (2014). A deglacial palaeomagnetic master curve for Fennoscandia—Providing a dating template and supporting millennial-scale geomagnetic field patterns for the past 14 ka. *Quaternary Science Reviews*, *106*, 155–166. https://doi.org/10.1016/j.quascirev.2014.03.008

Lund, S. (1996). A comparison of Holocene paleomagnetic secular variation records from North America. *Journal of Geophysical Research*, *101*(B4), 8007–8024. https://doi.org/10.1029/95JB00039

Lund, S., Keigwin, L., & Darby, D. (2016). Character of Holocene paleomagnetic secular variation in the tangent cylinder: Evidence from the Chukchi Sea. *Physics of the Earth and Planetary Interiors*, *256*, 49–58. https://doi.org/10.1016/j.pepi.2016.03.005

Lund, S., Oppo, D., & Curry, W. (2017). Late Quaternary paleomagnetic secular variation recorded in deep-sea sediments from the Demerara Rise, equatorial west Atlantic Ocean. *Physics of the Earth and Planetary Interiors*, *272*, 17–26. https://doi.org/10.1016/j.pepi.2017.04.010

Maenaka, K. (1990). Archaeomagnetic secular variation in South West Japan. *Rock Magnetism and Paleogeophysics*, *17*, 21–25.

Mankinen, E. A., & Champion, D. E. (1993). Broad trends in geomagnetic paleointensity on Hawaii during Holocene time. *Journal of Geophysical Research*, *98*(B5), 7959–7976. https://doi.org/10.1029/93JB00024

Mingram, J., Negendank, J. F., Brauer, A., Berger, D., Hendrich, A., Köhler, M., & Usinger, H. (2007). Long cores from small lakes—Recovering up to 100 m-long lake sediment sequences with a high-precision rod-operated piston corer (Usinger-corer). *Journal of Paleolimnology*, *37*(4), 517–528. https://doi.org/10.1007/s10933-006-9035-4

Mingram, J., Schettler, G., Nowaczyk, N., Luo, X. J., Lu, H. Y., Liu, J. Q., & Negendank, J. F. W. (2004). The Huguang maar lake-a high-resolution record of palaeoenvironmental and palaeoclimatic changes over the last 78,000 years from South China. *Quaternary International*, *122*(1), 85–107. https://doi.org/10.1016/j.quaint.2004.02.001

Mitra, R., Tauxe, L., & McIntosh, S. K. (2013). Two thousand years of archeointensity from West Africa. *Earth and Planetary Science Letters*, *364*, 123–133. https://doi.org/10.1016/j.epsl.2012.12.027

Nilsson, A., Holme, R., Korte, M., Suttie, N., & Hill, M. (2014). Reconstructing Holocene geomagnetic field variation: New methods, models and implications. *Geophysical Journal International*, *198*(1), 229–248. https://doi.org/10.1093/gji/ggu120

Noël, M., & Batt, C. M. (1990). A method for correcting geographically separated remanence directions for the purpose of archaeomagnetic dating. *Geophysical Journal International*, *102*(3), 753–756. https://doi.org/10.1111/j.1365-246X.1990.tb04594.x

Ojala, A. E. K., & Tiljander, M. (2003). Testing the fidelity of sediment chronology: Comparison of varve and paleomagnetic results from Holocene lake sediments from central Finland. *Quaternary Science Reviews*, *22*(15-17), 1787–1803. https://doi.org/10.1016/S0277-3791(03)00140-9

Oldfield, F. (1994). Toward the discrimination of fine-grained ferrimagnets by magnetic measurements in lake and near-shore marine sediments. *Journal of Geophysical Research*, *99*(B5), 9045–9050. https://doi.org/10.1029/93JB03137

Panovska, S., Korte, M., Finlay, C. C., & Constable, C. G. (2015). Limitations in paleomagnetic data and modelling techniques and their impact on Holocene geomagnetic field models. *Geophysical Journal International*, *202*(1), 402–418. https://doi.org/10.1093/gji/ggv137

Pavón-Carrasco, F. J., Osete, M. L., & Torta, J. M. (2010). Regional modeling of the geomagnetic field in Europe from 6000 to 1000 B.C. *Geochemistry, Geophysics, Geosystems*, *11*, Q11008. https://doi.org/10.1029/2010GC003197

Peck, J. A., King, J. W., Colman, S. M., & Kravchinsky, V. A. (1996). An 84-kyr paleomagnetic record from the sediments of Lake Baikal, Siberia. *Journal of Geophysical Research*, *101*(B5), 11,365–11,385. https://doi.org/10.1029/96JB00328

Pressling, N., Laj, C., Kissel, C., Champion, D., & Gubbins, D. (2006). Palaeomagnetic intensities from ^{14}C-dated lava flows on the Big Island, Hawaii: 0–21 kyr. *Earth and Planetary Science Letters*, *247*(1-2), 26–40. https://doi.org/10.1016/j.epsl.2006.04.026

Roberts, A. P., Pike, C. R., & Verosub, K. L. (2000). First-order reversal curve diagrams: A new tool for characterizing the magnetic properties of natural samples. *Journal of Geophysical Research*, *105*(B12), 28,461–28,475. https://doi.org/10.1029/2000JB900326

Shaar, R., Tauxe, L., Ron, H., Ebert, Y., Finkelstein, I., & Agnon, A. (2016). Large geomagnetic field anomalies revealed in Bronze to Iron Age archeomagnetic data from Tel Megiddo and Tel Hazor, Israel. *Earth and Planetary Science Letters*, *442*, 173–185. https://doi.org/10.1016/j.epsl.2016.02.038

Sheng, M., Wang, X., Zhang, S., Chu, G., Su, Y., & Yang, Z. (2017). A 20,000-year high-resolution pollen record from Huguangyan Maar Lake in tropical–subtropical South China. *Palaeogeography, Palaeoclimatology, Palaeoecology*, *472*, 83–92. https://doi.org/10.1016/j.palaeo.2017.01.038

Snowball, I., & Sandgren, P. (2004). Geomagnetic field intensity changes in Sweden between 9000 and 450 cal BP: Extending the record of "archaeomagnetic jerks" by means of lake sediments and the pseudo-Thellier technique. *Earth and Planetary Science Letters*, *227*(3-4), 361–376. https://doi.org/10.1016/j.epsl.2004.09.017

Stanton, T., Nilsson, A., Snowball, I., & Muscheler, R. (2011). Assessing the reliability of Holocene relative palaeointensity estimates: A case study from Swedish varved lake sediments. *Geophysical Journal International*, *187*(3), 1195–1214. https://doi.org/10.1111/j.1365-246X.2011.05049.x

Stanton, T., Snowball, I., Zillén, L., & Wastegård, S. (2010). Validating a Swedish varve chronology using radiocarbon, palaeomagnetic secular variation, lead pollution history and statistical correlation. *Quaternary Geochronology*, *5*(6), 611–624. https://doi.org/10.1016/j.quageo.2010.03.004

Stoner, J. S., Channell, J. E. T., Mazaud, A., Strano, S. E., & Xuan, C. (2013). The influence of high-latitude flux lobes on the Holocene paleomagnetic record of IODP Site U1305 and the northern North Atlantic. *Geochemistry, Geophysics, Geosystems*, *14*, 4623–4646. https://doi.org/10.1002/ggge.20272

St-Onge, G., Stoner, J. S., & Hillaire-Marcel, C. (2003). Holocene paleomagnetic records from the St. Lawrence Estuary, eastern Canada: Centennial- to millennial-scale geomagnetic modulation of cosmogenic isotopes. *Earth and Planetary Science Letters*, *209*(1-2), 113–130. https://doi.org/10.1016/S0012-821X(03)00079-7

Tauxe, L. (1993). Sedimentary records of relative paleointensity of the geomagnetic field: Theory and practice. *Reviews of Geophysics*, *31*(3), 319–354. https://doi.org/10.1029/93RG01771

Tema, E., & Kondopoulou, D. (2011). Secular variation of the Earth's magnetic field in the Balkan region during the last eight millennia based on archaeomagnetic data. *Geophysical Journal International*, *186*(2), 603–614. https://doi.org/10.1111/j.1365-246X.2011.05088.x

Thompson, R., & Oldfield, F. (1986). *Environmental Magnetism*, (pp. 1–127). London: Allen & Unwin. https://doi.org/10.1007/978-94-011-8036-8

Thompson, R., Stober, J. C., Turner, G. M., Oldfield, F., Bloemendal, J., Dearing, J. A., & Rummery, T. A. (1980). Environmental applications of magnetic measurements. *Science*, *207*(4430), 481–486. https://doi.org/10.1126/science.207.4430.481

Thouveny, N., & Williamson, D. (1988). Paleomagnetic study of the Holocene and upper Pleistocene sediments from lake Barombi Mbo, Cameroun: First results. *Physics of the Earth and Planetary Interiors*, *52*(3-4), 193–206. https://doi.org/10.1016/0031-9201(88)90115-X

Turner, G. M., & Thompson, R. (1981). Lake sediment record of the geomagnetic secular variation in Britain during Holocene times. *Geophysical Journal International*, *65*(3), 703–725. https://doi.org/10.1111/j.1365-246X.1981.tb04879.x

Valet, J. P., Tric, E., Herrero-Bervera, E., Meynadier, L., & Lockwood, J. P. (1998). Absolute paleointensity from Hawaiian lavas younger than 35 ka. *Earth and Planetary Science Letters*, *161*(1-4), 19–32. https://doi.org/10.1016/S0012-821X(98)00133-2

Wang, X., Chu, G., Sheng, M., Zhang, S., Li, J., Chen, Y., et al. (2016). Millennial-scale Asian summer monsoon variations in South China since the last deglaciation. *Earth and Planetary Science Letters*, *451*, 22–30. https://doi.org/10.1016/j.epsl.2016.07.006

Wei, Q. Y., Li, D. J., Cao, G. Y., Zhang, W. S., & Wang, S. P. (1981). Secular variation of the direction of the ancient geomagnetic field records for Loyang region, China. *Physics of the Earth and Planetary Interiors*, *25*(1), 107–112. https://doi.org/10.1016/0031-9201(81)90132-1

Wu, X. D., Wang, Y., Bian, L., & Shen, J. (2016). Diagenetic effects on magnetic minerals in a Holocene lacustrine sediment core from Huguangyan maar lake, southeast China. *Geophysical Journal International*, *206*(3), 1586–1598. https://doi.org/10.1093/gji/ggw223

Wu, X. D., Zhang, Z. H., Xu, X. M., & Shen, J. (2012). Asian summer monsoonal variations during the Holocene revealed by Huguangyan maar lake sediment record. *Palaeogeography, Palaeoclimatology, Palaeoecology*, *323-325*, 13–21. https://doi.org/10.1016/j.palaeo.2012.01.020

Yancheva, G., Nowaczyk, N. R., Mingram, J., Dulski, P., Schettler, G., Negendank, J. F., et al. (2007). Influence of the intertropical convergence zone on the East Asian monsoon. *Nature*, *445*(7123), 74–77. https://doi.org/10.1038/nature05431

Yang, X., Heller, F., Yang, J., & Su, Z. (2009). Paleosecular variations since ~9000 yr BP as recorded by sediments from maar lake Shuangchiling, Hainan, South China. *Earth and Planetary Science Letters*, *288*(1-2), 1–9. https://doi.org/10.1016/j.epsl.2009.07.023

Yang, X., Liu, Q., Duan, Z., Su, Z., Wei, G., Jia, G., et al. (2012). A Holocene palaeomagnetic secular variation record from Huguangyan maar Lake, southern China. *Geophysical Journal International*, *190*(1), 188–200. https://doi.org/10.1111/j.1365-246X.2012.05475.x

Yang, X., Liu, Q., Yu, K., Huang, W., Zhu, L., Zhang, H., et al. (2016). Paleosecular variations of the geomagnetic field during the Holocene from Eastern Asia. *Physics of the Earth and Planetary Interiors*, *254*(25-36), 25–36. https://doi.org/10.1016/j.pepi.2016.03.004

Yu, Y. (2012). High-fidelity paleointensity determination from historic volcanoes in Japan. *Journal of Geophysical Research*, *117*, B08101. https://doi.org/10.1029/2012JB009368

Yu, Y., Doh, S.-J., Kim, W., Park, Y.-H., Lee, H.-J., Yim, Y., et al. (2010). Archeomagnetic secular variation from Korea: Implication for the occurrence of global archeomagnetic jerks. *Earth and Planetary Science Letters*, *294*(1-2), 173–181. https://doi.org/10.1016/j.epsl.2010.03.024

Zheng, Y., Zheng, H., Deng, C., & Liu, Q. (2014). Holocene paleomagnetic secular variation from East China Sea and a PSV stack of East Asia. *Physics of the Earth and Planetary Interiors*, *236*, 69–78. https://doi.org/10.1016/j.pepi.2014.07.001